PROCEEDINGS OF SCIENCE

Search for rare decays of the Higgs boson with the ATLAS detector

Artem Basalaev*on behalf of the ATLAS Collaboration

Deutsches Elektronen-Synchrotron (DESY),
Notkestrasse 85, Hamburg, Germany

E-mail: artem.basalaev@desy.de

The Standard Model predicts several rare Higgs boson decay channels, some of which are currently within experimental reach. Among these is the decay to a lepton pair and a photon, $H \to \ell\ell\gamma$ ($\ell = e, \mu$). The observation of this decay could open the possibility of studying the CP and coupling properties of the Higgs boson in a complementary way to other analyses. Two distinct regimes with different lepton pair invariant masses are explored: low lepton pair mass ($m_{\ell\ell} < 30$ GeV), where the decay predominantly occurs through the virtual photon, γ^*, and intermediate lepton pair mass (in a window around $m_{\ell\ell} = 91.2$ GeV), where the decay predominantly occurs through the Z boson. Results are based on 139 fb^{-1} of pp collision data at 13 TeV center-of-mass energy collected with the ATLAS detector at the Large Hadron Collider. An upper limit at 95% confidence level on the production cross-section times branching ratio for $pp \to H \to Z\gamma$ is set at 3.6 times the Standard Model prediction (with 2.6 times expected in the presence of the Standard Model Higgs boson). An excess over the background-only hypothesis is observed in the $m_{\ell\ell} < 30$ GeV regime at 3.2σ significance (2.1σ expected), establishing evidence for the $H \to \ell\ell\gamma$ decay. The Higgs boson production cross-section times $H \to \ell\ell\gamma$ branching ratio for $m_{\ell\ell} < 30$ GeV is measured to be $8.7^{+2.8}_{-2.7}$ fb.

*** *The European Physical Society Conference on High Energy Physics (EPS-HEP2021),* ***
*** *26-30 July 2021* ***
*** *Online conference, jointly organized by Universität Hamburg and the research center DESY* ***

*Speaker

PoS(EPS-HEP2021)599

1. Introduction

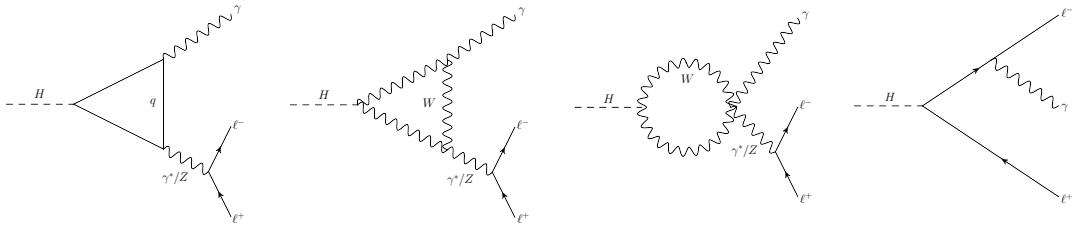

Figure 1: Representative Feynman diagrams for the $H \to \ell\ell\gamma$ decay [1].

A particle consistent with the properties of the Standard Model (SM) Higgs boson was discovered by the ATLAS and CMS collaborations in 2012 [2, 3]. Since then, it has been independently observed with a significance of more than 5σ in the $H \to b\bar{b}$, $H \to WW^* \to e\nu\mu\nu$, $H \to \tau\tau$, $H \to ZZ^* \to \ell^+\ell^-\ell^+\ell^-$, and $H \to \gamma\gamma$ decay channels. The efforts to study properties of the Higgs boson in different decay channels continue, and with the full data set from the second run (2015-2018) of the Large Hadron Collider (LHC) it becomes possible to explore rarer decays. Among the recent highlights is the $H \to \mu\mu$ decay, for which evidence at 3.0σ significance has been established by the CMS collaboration [4].

A rare Higgs boson decay to a lepton pair and a photon, $H \to \ell\ell\gamma$ ($\ell = e, \mu$), is explored in this report. This three-body decay can be used to probe CP violation in the Higgs sector in future measurements [5, 6]. In addition, it may be sensitive to coupling modifications introduced by possible extensions to the SM [7]. The representative Feynman diagrams for the $H \to \ell\ell\gamma$ decay are shown in Figure 1. The decay typically features a quark or a vector boson loop, with a very small contribution from tree-level diagrams in the explored kinematic region [8]. In the low lepton-pair invariant mass regime the decay predominantly occurs through the virtual photon, γ^*. This regime is explored in the low-$m_{\ell\ell}$ $H \to \ell\ell\gamma$ search ($m_{\ell\ell} < 30$ GeV). The decay predominantly through the Z boson, where the lepton pair mass is in the vicinity of $m_Z = 91.2$ GeV, is explored in the $H \to Z\gamma$ search. The branching ratio $BR(H \to Z\gamma)$ is predicted to be 1.541×10^{-3} [9]. For the lepton pair masses $m_{\ell\ell} < 30$ GeV, the branching ratios for the $ee\gamma$ and $\mu\mu\gamma$ channels, as estimated with `Pythia 8`, correspond to $BR(H \to ee\gamma) = 7.20 \times 10^{-5}$ and $BR(H \to \mu\mu\gamma) = 3.42 \times 10^{-5}$ [1], respectively. The Higgs boson mass is assumed to be $m_H = 125.09$ GeV in all branching ratio calculations.

In previously published reports, the observed 95% confidence level (CL) upper limit on the production cross-section times branching ratio for the $pp \to H \to Z\gamma$ process was set at 7.4 times [10] (6.6 times [11]) the SM prediction by CMS (ATLAS) collaborations, using 35.9 (36.1) fb^{-1}of collision data. The CMS Collaboration additionally reported a 95% CL upper limit on the Higgs boson production cross-section times the $H \to \mu\mu\gamma$ branching ratio of 4.0 times [10] the SM prediction for the low muon pair invariant mass regime ($m_{\mu^+\mu^-} < 50$ GeV) with the same data set. The presented results [1, 12] are based on 139 fb^{-1} of pp collision data at 13 TeV center-of-mass energy collected with the ATLAS detector [13] during the second run of the LHC.

2. Search for $H \to Z\gamma \to \ell\ell\gamma$ decays

In this analysis, the events are required to contain a photon candidate and at least two oppositely-charged electron or muon candidates. The candidate lepton pair must be associated with the primary vertex, which is defined as the vertex with the largest sum of the squared transverse momenta of the associated charged particle tracks in the inner detector (ID). Muon candidates are reconstructed from high-quality tracks in the muon spectrometer (MS) and ID. Muon candidates are typically required to have matching tracks in the MS and the ID. Outside of the ID acceptance, muon candidates with the track only in the MS are also accepted, provided the track points to the beamspot. Reconstruction of the electron and photon candidates is based on topological clusters of energy deposits in the electromagnetic calorimeter. Electron candidates are required to have a track in the ID that is matched to the cluster. Photon candidates with a track or conversion vertex matched to the cluster are categorized as converted. Additional identification criteria are imposed on the lepton and photon candidates as well as a requirement to be well-isolated from additional activity in both the tracking detector and the calorimeters. Jets are reconstructed using the anti-k_t algorithm with a radius parameter of 0.4. To suppress backgrounds, most notably those from pileup interactions, candidate objects are required to satisfy additional kinematic requirements. Close-by objects are rejected with an overlap removal procedure to avoid double-counting.

The selected lepton pair forms a Z candidate. In the case of the muon pair, nearby energy deposits consistent with final-state photon radiation are added to the Z candidate momentum to improve the Z boson mass resolution. A constrained kinematic fit based on previous measurements of the invariant mass of the Z boson is used to correct the four-momenta of the lepton pair. The lepton pair invariant mass is required to be within 10 GeV of the Z boson mass, $m_Z = 91.2$ GeV. The Z boson candidate and the highest-p_{T} photon in the event form the Higgs boson candidate, provided that the photon p_{T} relative to the three-body invariant mass of the Higgs boson candidate $m_{Z\gamma}$ satisfies $p_{\mathrm{T}}^{\gamma}/m_{Z\gamma} > 0.12$. Higgs boson candidates in the 105 GeV $< m_{Z\gamma} <$ 160 GeV mass range are considered, to provide sufficient phase space to constrain remaining backgrounds.

To improve the sensitivity of the search, selected events are classified into mutually exclusive categories based on the expected signal-to-background ratio and $m_{Z\gamma}$ resolution. In particular the events where the Higgs boson is produced via vector boson fusion (VBF) are expected to have a higher signal-to-background ratio. A boosted decision tree (BDT) is trained on a subset of kinematic variables to define a VBF-enhanced category. In total, six categories are defined according to the lepton flavor and event kinematics.

The remaining background mainly originates from non-resonant SM $Z\gamma$, with a small contribution from the production of Z bosons in association with jets, where one jet is misidentified as a photon. Parametric models of the three-body invariant mass distributions in each category are constructed. The signal contribution is modelled with a double-sided Crystal Ball (DSCB) function, featuring a Gaussian core and asymmetric power-law tails. The expected acceptance and parameters that describe the shape of the signal are obtained from Monte-Carlo (MC) simulated events. The background contribution is modelled with a simple function, chosen using a template constructed from simulated background events with the composition determined from a data-driven fit. The resulting combined signal-plus-background model is then fit to data, where the remaining parameters are determined.

3. Search for low-$m_{\ell\ell}$ $H \to \ell\ell\gamma$ decays

The analysis strategy is similar to that of the $H \to Z\gamma$ search, but in the $m_{\ell\ell} < 30$ GeV region there are several kinematic features in a typical event that require different treatment. In this phase space, events typically feature highly collimated leptons; for electrons, this means that the corresponding EM calorimeter deposits often merge. Already in data taking, trigger efficiencies of traditional electron triggers are significantly reduced for such ee-merged events. To counteract this, a dedicated trigger was employed in the 2017 and 2018 data taking periods, featuring an upper threshold on hadronic leakage in the calorimeter, but no requirement on the width of the shower. Merged electrons are subsequently reconstructed by matching two tracks to a single EM topocluster. The energy calibration for converted photons with $r = 30$ mm is used to calibrate the energy of the merged electrons, due to their kinematic similarities. At the same time, additional track requirements are applied to merged electron candidates to suppress converted photons in the signal region. A multivariate discriminator is trained to separate ee-merged events from jet backgrounds. The identification and isolation efficiency in data reaches $\sim 50\%$, measured using a tag-and-probe method with $Z \to \ell\ell\gamma$ events.

The candidate events are further selected using several kinematic requirements to suppress backgrounds, including $p_{\mathrm{T}}^{\gamma}/m_{\ell\ell\gamma} > 0.3$ and $p_{\mathrm{T}}^{\ell\ell}/m_{\ell\ell\gamma} > 0.3$. The events in the 110 GeV $< m_{\ell\ell\gamma} <$ 160 GeV mass range are subsequently categorized in the following mutually exclusive categories (ordered by priority): targeting the VBF production mode, high-$p_{\mathrm{TThrust}}^{\ell\ell\gamma}$ [1], and low-$p_{\mathrm{TThrust}}^{\ell\ell\gamma}$ events. With further separation into ee-resolved, ee-merged and $\mu\mu$ events, this results in nine categories total.

The signal-plus-background model is constructed using the same approach as for the $H \to Z\gamma$ analysis. One difference is that a very small resonant background from $H \to \gamma\gamma$ exists in the electron categories, caused by one converted photon being misidentified as an electron pair. Its contribution is modelled using the DSCB function from the signal fit normalized to the expected $H \to \gamma\gamma$ yield from MC simulation.

4. Results

In both searches, systematic uncertainties mainly arise from the bias associated with the choice of the background fitting function, calculation of the branching ratios, and missing higher-order corrections in QCD. Other theory and experimental uncertainties are also considered, but have a much smaller impact. Both results are dominated by statistical uncertainties. In Figure 2 (a) the three-body invariant mass distribution for the $H \to Z\gamma$ search is shown, and in Figure 2 (b) for the low-$m_{\ell\ell}$ $H \to \ell\ell\gamma$ search, with every data event reweighted by a category-dependent weight to visually highlight sensitivity of respective searches.

In the $H \to Z\gamma$ search, the best-fit value for the signal strength is found to be $\mu_{Z\gamma} = 2.0 \pm 0.9(\mathrm{stat.})^{+0.4}_{-0.3}(\mathrm{syst.}) = 2.0^{+1.0}_{-0.9}(\mathrm{tot.})$ with an expected value of $\mu_{Z\gamma,\mathrm{exp}} = 1.0 \pm 0.8(\mathrm{stat.}) \pm 0.3(\mathrm{syst.})$. The observed 95% CL limit on the signal strength is found to be 3.6 times the SM prediction compared with the expected value of 2.6 assuming the SM Higgs boson.

[1] $p_{\mathrm{TThrust}}^{\ell\ell\gamma} = |\vec{p}_{\mathrm{T}}^{\,\ell\ell\gamma} \times \hat{t}|$, where $\hat{t} = (\vec{p}_{\mathrm{T}}^{\,\ell\ell} - \vec{p}_{\mathrm{T}}^{\,\gamma})/|\vec{p}_{\mathrm{T}}^{\,\ell\ell} - \vec{p}_{\mathrm{T}}^{\,\gamma}|$. This quantity is strongly correlated with the $\vec{p}_{\mathrm{T}}^{\,\ell\ell\gamma}$.

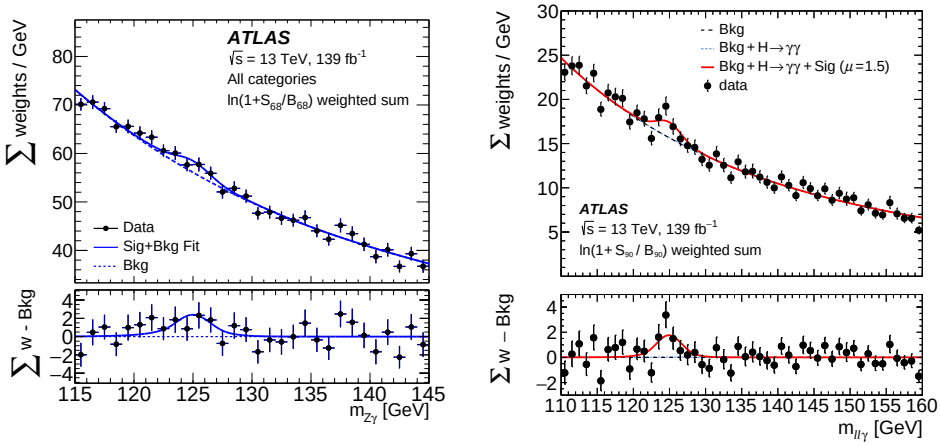

(a) (b)

Figure 2: The three-body invariant mass distribution for the $H \to Z\gamma$ search (a) [12] and for the low-$m_{\ell\ell}$ $H \to \ell\ell\gamma$ search (b) [1], with every data event (black circles) reweighted by a category-dependent weight, $\ln(1 + S_X/B_X)$, where S_X is the number of signal events in the smallest window containing X% of the expected signal (68% for the $H \to Z\gamma$ search and 90% for the low-$m_{\ell\ell}$ $H \to \ell\ell\gamma$ search), and B_X is the expected number of background events in the same window. The solid curve shows the combined $S + B$ model when fitting all analysis categories simultaneously, the dashed line shows the model of the non-resonant background component and (only for the low-$m_{\ell\ell}$ search) the dotted line denotes the sum of the non-resonant background and the resonant $H \to \gamma\gamma$ background. The bottom panel shows the residuals of the data with respect to the non-resonant background component of the $S + B$ fit.

In the low-$m_{\ell\ell}$ $H \to \ell\ell\gamma$ search, the best-fit value for the signal strength is found to be $\mu_{\text{low-}m_{\ell\ell}} = 1.5 \pm 0.5(\text{stat.})^{+0.2}_{-0.1}(\text{syst.}) = 1.5 \pm 0.5(\text{tot.})$ with an expected value of $\mu_{\text{low-}m_{\ell\ell},\text{exp}} = 1.0 \pm 0.5(\text{stat.})^{+0.2}_{-0.1}(\text{syst.})$. This corresponds to an excess with a 3.2σ significance over the background-only hypothesis, compared to an expected significance of 2.1σ. Additionally, the Higgs boson production cross-section times the $H \to \ell\ell\gamma$ branching ratio for $m_{ll} < 30$ GeV is determined to be $8.7^{+2.8}_{-2.7}$ fb. In this result, only the theoretical systematic uncertainties associated with the acceptance remain, and the uncertainties in the predicted cross-sections and branching ratio do not apply.

The 3.2σ significance of excess constitutes the first evidence for the $H \to \ell\ell\gamma$ decay. The two searches presented are statistically limited, with results expected to improve considerably with more data. This result is an important step towards probing Higgs boson couplings and CP properties in this rare decay channel.

References

[1] ATLAS Collaboration, *Evidence for Higgs boson decays to a low-mass dilepton system and a photon in pp collisions at $\sqrt{s} = 13$ TeV with the ATLAS detector*, *Phys. Lett. B* **819** (2021) 136412.

[2] ATLAS Collaboration, *Observation of a new particle in the search for the Standard Model Higgs boson with the ATLAS detector at the LHC*, *Phys. Lett. B* **716** (2012) 1 .

[3] CMS Collaboration, *Observation of a new boson at a mass of 125 GeV with the CMS experiment at the LHC*, *Phys. Lett. B* **716** (2012) 30 .

[4] CMS Collaboration, *Evidence for Higgs boson decay to a pair of muons*, *JHEP* **01** (2021) 148 [2009.04363].

[5] A. Korchin and V. Kovalchuk, *Polarization effects in the Higgs boson decay to Z and test of CP and CPT symmetries*, *Phys. Rev. D* **88** (2013) 036009.

[6] Y. Chen, A. Falkowski, I. Low and R. Vega-Morales, *New observables for CP violation in Higgs decays*, *Phys. Rev. D* **90** (2014) 113006 [1405.6723].

[7] A. Kachanovich, U. Nierste and I. Nišandžić, *Higgs boson decay into a lepton pair and a photon revisited*, *Phys. Rev. D* **101** (2020) 073003 [2001.06516].

[8] Y. Sun, H. Chang and D. Gao, *Higgs decays to $\gamma\,\ell^+\ell^-$ in the standard model*, *J. High Energy Phys.* **61** (2013) .

[9] LHC Higgs Cross Section Working Group collaboration, *Handbook of LHC Higgs Cross Sections: 4. Deciphering the Nature of the Higgs Sector*, 1610.07922.

[10] CMS Collaboration, *Search for the decay of a Higgs boson in the $ll\gamma$ channel in proton-proton collisions at $\sqrt{s}$ = 13 TeV*, *JHEP* **11** (2018) 152 [1806.05996].

[11] ATLAS Collaboration, *Search for the $Z\gamma$ decay mode of the Higgs boson and for new high-mass resonances in pp collisions at $\sqrt{s}$ = 13 TeV with the ATLAS detector*, *JHEP* **10** (2017) 112 [1708.00212].

[12] ATLAS Collaboration, *A search for the $Z\gamma$ decay mode of the Higgs boson in pp collisions at $\sqrt{s}$ = 13 TeV with the ATLAS detector*, *Phys. Lett. B* **809** (2020) 135754.

[13] ATLAS Collaboration, *The ATLAS experiment at the CERN Large Hadron Collider*, *JINST* **3** (2008) S08003.

PoS(EPS-HEP2021)599